Structure of Self-Assembled Monolayers of Semifluorinated Alkanethiols on Gold and Silver Substrates

S. Frey,[a] K. Heister,[a] M. Zharnikov,[a,*] M. Grunze,[a] K. Tamada,[b] R. Colorado, Jr.,[c] M. Graupe,[c] O. E. Shmakova,[c] and T. R. Lee[c]

[a]*Angewandte Physikalische Chemie, Universität Heidelberg, Im Neuenheimer Feld 253, 69120 Heidelberg, Germany*

[b]*National Institute of Materials and Chemical Research, Tsukuba, Ibaraki 305, Japan*

[c]*Department of Chemistry, University of Houston, Houston, Texas 77204-5641, USA*

(Received 13 March 2000)

Abstract. Self-assembled monolayers (SAMs) formed from semifluorinated alkanethiols (SFATs) $CF_3(CF_2)_9(CH_2)_nSH$ (F10HnSH: n = 2, 11, and 17) on polycrystalline Au and Ag were characterized by X-ray photoelectron spectroscopy, infrared reflection absorption spectroscopy, and near edge X-ray absorption fine structure spectroscopy. SFATs were found to form highly ordered and densely packed SAMs on both substrates. The molecules are strongly bonded to the substrates via their sulfur head groups, in the same manner as conventional alkanethiol (AT) SAMs. The hydrocarbon (except for n = 2) and fluorocarbon parts of the adsorbed SFATs retain the expected planar zigzag and helical conformations of the respective bulk materials. The orientation of the fluorocarbon chains does not depend on the substrate. These entities are almost perpendicular to the substrate in F10H2S/Au and F10H2S/Ag and become slightly more tilted in SFAT SAMs with longer hydrocarbon moieties. However, the alkyl parts of the SFAT films exhibit tilt and twist angles that are similar to those of normal alkanethiol films on Ag and Au substrates despite the reduced packing density in the SFAT films as compared to normal AT SAMs. We suggest that the substrate-related differences in tilt and twist angles for both systems are associated with the different character of the headgroup–substrate bonding on Au and Ag.

1. INTRODUCTION

During the last two decades, self-assembled monolayers (SAMs) have attracted considerable interest because of their potential application to control wetting, adhesion, lubrication, and corrosion on surfaces and interfaces.[1-3] SAMs are close-packed arrays of chain- or rod-like molecules that are chemically anchored to a suitable substrate. Generally, these molecules consist of three parts: a head group that binds strongly to the substrate, a tail group that constitutes the outer surface of the film, and a spacer that connects head and tail and influences the intermolecular spacing, molecular orientation, and the degree of order in the film. Providing that the tail group has strong polar character and/or large steric bulk, it can influence both the interfacial properties and the internal structural properties of the film.

One such system is semifluorinated alkanethiols (SFATs) $CF_3(CF_2)_{m-1}(CH_2)_nSH$ (FmHnSH), which are basically alkanethiols (ATs) with fluorocarbon tail groups. In a SFAT molecule, a hydrocarbon segment is terminated by a fluorocarbon chain. The physical and chemical properties of these entities are unique, which stems from the larger atomic volume and higher electronegativity of fluorine relative to hydrogen. When compared to hydrocarbon chains, fluorocarbon chains are more hydrophobic, stiffer, and possess a larger molecular volume: The van der Waals (vdW) diameter of perfluorocarbon chains is 5.6 Å,[4] compared to 4.2 Å[4] for hydrocarbon chains. The larger volume is essentially caused by the helical conformation of the fluorocarbon chains, which is characteristic of bulk materials such as poly(tetra-fluoroethylene) (PTFE), whereas the hydrocarbon chains typically have a planar zigzag conformation [e.g., in poly(ethylene) (PE)]. The helical conformation

*Author to whom correspondence should be addressed. E-mail: michael.zharnikov@urz.uni-heidelberg.de

of fluorocarbon chains occurs via rotation about the C–C bonds, which arises from dipolar repulsion between 1,3-diaxial C–F bonds.[5] The twist angle is about 12°–15° per C–C bond, and the dihedral angle between adjacent planes of three neighboring carbon atoms is 160°–165°.[6-8]

Until now, most studies of SFAT SAMs have relied on the adsorption of SFATs having short hydrocarbon parts (e.g., FnH2SH) onto gold substrates consisting of predominantly (111) facets.[9-12] These films were found to be well-ordered and densely packed. AFM and X-ray diffraction data revealed an enlarged (relative to AT SAMs) intermolecular spacing of ≈5.8 Å,[9-12] which is consistent with a model in which the fluorocarbon parts retain the helical conformation of bulk fluorocarbon chains. This assumption was supported by IR analysis, where the characteristic adsorption modes assigned to the helical conformation were observed.[9,11] For the hydrocarbon chains of F8H11S/Au, a planar all-trans conformation was found.[11] For FnH2S/Au (n = 6, 8, 12), the average tilt angle of the fluorocarbon chains was estimated to be 12°–20°,[9,10] and for F8H11S/Au, the average tilt angle of the hydrocarbon chain was assumed to be less than that for normal AT SAMs.[11] Also, SAMs formed from alkyl fluoroalkyl disulfides and semifluorinated amidethiols were studied.[13-15] The results cannot, however, be directly compared to those for SAMs consisting exclusively of hydrocarbon and fluorocarbon chains because the additional functional groups can influence the structure of the SAMs.

Thus, there is a definite lack of information regarding the structure of SFAT films possessing long hydrocarbon segments. Another interesting aspect, which has not been touched upon until now, is the structure of the SFAT SAMs on different substrates, such as silver. It is well-known that both the lateral density and hence the tilt and twist angles of AT SAMs on gold and silver are different. This fact is commonly regarded to reflect a sensitive balance between head-group–substrate, intermolecular vdW, and intramolecular interactions.[16] Favorable intermolecular interactions are maximized when alkyl chains pack in a trigonal lattice with interchain distances near ≈4.4 Å and are oriented normal to the substrate surface.[2,4] This is nearly achieved in AT SAMs on Ag, where the small corrugation of the binding energy surface results in a packing of the sulfur head groups (thiolates) that permits a close packing of the alkyl chains: A 2D lattice constant of ≈4.67–4.77 Å and an average tilt angle of 10°–12° were found in this system.[1,2,17-19] The situation is different in the case of AT/Au(111) SAMs, where the anchoring thiolates occupy hollow sites with intersite spacings of ≈5.0 Å, which prevents effective packing of trans-extended alkyl chains oriented normal to the surface.[2] To maximize interchain vdW interactions, the AT molecules tilt from the surface normal: an average tilt angle of 27°–35° (depending on the technique used)[20] is observed for AT SAMs on Au(111), which corresponds to interchain distances of approximately 4.4 Å.[17,21-23]

In SFAT SAMs, the intermolecular spacing between the alkyl chains is expected to be larger than that in normal AT SAMs due to the bulky fluorocarbon tail groups. Thus, we were interested in determining how the alkyl chains are tilted and twisted in light of the anticipated increased interchain distances. To this end, we have investigated the structure of SFAT SAMs formed on polycrystalline Au and Ag from F10HnSH with n = 2, 11, and 17. The objectives of this study were to determine the individual conformation and orientation of the hydro- and fluorocarbon parts of the SFAT molecules on both Au and Ag surfaces.

The properties of the SFAT films were monitored by infrared reflection absorption spectroscopy (IRRAS), X-ray photoelectron spectroscopy (XPS), and near edge X-ray adsorption fine structure (NEXAFS) spectroscopy. These techniques are complementary tools for the investigation of thin organic layers and, in particular, SAMs.

2. EXPERIMENTAL

The compound F10H2SH was prepared in pure form with spectral data consistent with those reported in the literature.[24] Compounds F10H11SH and F10H17SH were prepared using recently described methodologies.[25] Scheme 1a outlines the five-step synthesis used to prepare F10H11SH, and Scheme 1b illustrates the nine-step synthesis of F10H17SH. Experimental details and analytical data are provided below. All starting materials and reagents were of the highest purity available from commercial suppliers.

Synthesis of F10H11SH. A 50-mL Schlenk flask was filled with perfluorodecyl iodide (6.68 g, 10.3 mmol), 10-undecen-1-ol (1.70 g, 10.0 mmol), and the radical initiator 2,2'-azobisisobutyronitrile (AIBN; 0.03 g, 0.20 mmol). The flask was closed, evacuated until the reactants began to bubble, and refilled with argon. This process was repeated two additional times. After a final evacuation, the reaction mixture was stirred for 3 h at 90° C. After cooling the flask to room temperature, another portion of AIBN (0.03 g, 0.20 mmol) was added. The flask was again evacuated by the aforementioned method, and the mixture was then stirred at 90° C for an additional 3 h. Subsequent additions of radical initiator were continued until all of the 10-undecen-1-ol had reacted, as indicated by ^{1}H NMR spectroscopy. The flask was then cooled to room temperature, and the reaction mixture was dissolved with a mixture of 20 mL of tetrahydrofuran (THF) and 40 mL of acetic acid. Zinc dust (2.00 g, 30.6 mmol) was added to the flask, and the reaction mixture was stirred for 12 h at room

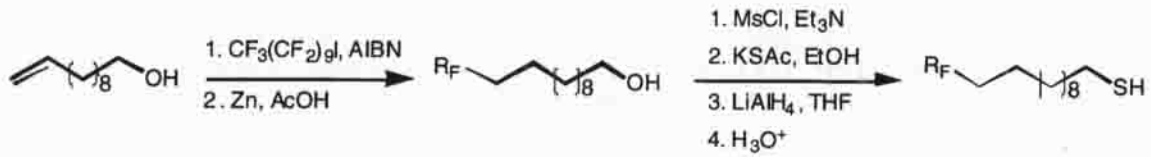

Scheme Ia. Synthesis of F10H11SH.

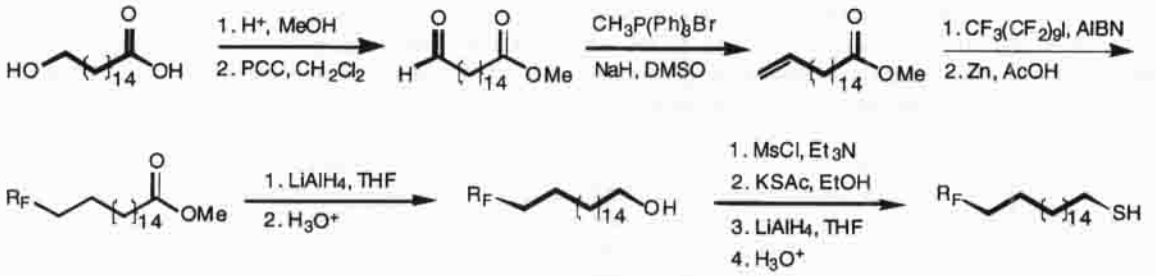

Scheme Ib. Synthesis of F10H17SH.

temperature. The mixture was then filtered through Celite. The Celite was rinsed with two 100-mL portions of diethyl ether, and the resulting clear solution was concentrated by rotary evaporation. The residue was dissolved in 200 mL of diethyl ether, and this ethereal solution was rinsed with equivalent volumes of satd aq $NaHCO_3$ and satd aq NaCl, dried with $MgSO_4$, and filtered. After removing the solvent by rotary evaporation, the crude product was purified by column chromatography on silica gel (2:1, hexanes:diethyl ether) to give 11-perfluorodecyl-1-undecanol (4.55 g, 6.60 mmol, 66% yield). ^{1}H NMR (300 MHz, $CDCl_3$): d 3.64 (t, J = 6.6 Hz, 2 H), 2.19–1.83 (m, 2 H), 1.67–1.45 (m, 5 H), 1.43–1.20 (m, 14 H).

11-Perfluorodecyl-1-undecanol (4.55 g, 6.60 mmol) was dissolved in a mixture of 100 mL of THF and 200 mL of hexanes. Triethylamine (2.00 g, 19.8 mmol) and methanesulfonyl chloride (1.51 g, 13.2 mmol) were added to the solution. The reaction mixture was stirred at room temperature for 2 h. Water (200 mL) was added to the organic mixture, and the organic phase was separated, rinsed with satd aq NaCl, dried with $MgSO_4$, and filtered. The solvent was removed by rotary evaporation to give the crude mesylate, which was subsequently dissolved in a mixture of 100 mL of THF and 200 mL of absolute ethanol. After adding potassium thioacetate (1.50 g, 13.2 mmol) to the solution, the mixture was stirred and refluxed for 2 h under argon. The reaction mixture was then cooled to room temperature, combined with 200 mL of water, and extracted with hexanes (3 × 200 mL). After combining the organic portions, the solution was rinsed with 200 mL of satd aq NaCl, dried with $MgSO_4$, and filtered. The solvent was removed by rotary evaporation to give the crude thioacetate, which was subsequently dissolved in 100 mL of THF. This solution was added, over 5 min, to a suspension of lithium aluminum hydride (0.50 g, 13.2 mmol) in 100 mL of THF. The mixture was then stirred and refluxed under argon for 2 h. The reaction was cooled to 0° C, and methanol was added dropwise until the evolution of hydrogen ceased. After adding 200 mL of water, concd HCl was added dropwise until the aqueous layer was acidic, as indicated by litmus paper. The mixture was extracted with diethyl ether (3 × 150 mL). The organic portions were combined and rinsed with 200 mL of water, satd aq $NaHCO_3$, and satd aq NaCl, dried with $MgSO_4$, and filtered. The solvent was removed by rotary evaporation to give the crude product, which was purified by column chromatography on silica gel (hexanes) to give 11-perfluorodecyl-1-undecanethiol (2.42 g, 3.43 mmol, 52% yield).Comprehensive analytical characterization of the final product is provided: (12,12,13,13,14,14,15,15,16,16,17,17,18,18,19,19,20,20,21,21,21-heneicosafluoro-1-heneicosanethiol; F10H11SH). ^{1}H NMR (300 MHz, $CDCl_3$): δ 2.50 (q, J = 7.2 Hz, 2 H), 2.17–1.92 (m, 2 H), 1.71–1.53 (m, 4 H), 1.48–1.22 (m, 15 H). ^{13}C NMR (75.5 MHz, $CDCl_3$): δ = 120–110 (bm, 10 C), 34.26, 31.15 (t, $^2J_{CF}$ = 23 Hz), 29.72 (2 C), 29.87, 29.45, 29.38, 29.31, 28.60, 24.89, 20.33. Broad resonances with chemical shifts in the range of δ 120–110 are characteristic of long perfluorocarbon chains.[26] Anal. Calc for $C_{21}H_{23}F_{21}S$: C, 35.70; H, 3.28. Found: C, 35.99; H, 3.65.

Synthesis of F10H17SH. 16-Hydroxyhexadecanoic acid (5.00 g, 18.4 mmol), trimethyl orthoformate (3.88 g, 36.7 mmol), and *p*-toluenesulfonic acid monohydrate (0.20 g, 1.05 mmol) were placed into a flask containing 30 mL of methanol. The resulting mixture was stirred at room temperature for 16 h. The solvent was then removed by rotary evaporation, and the residue was dissolved in 50 mL of hexanes. This solution was washed with equivalent volumes of satd aq $NaHCO_3$ and satd aq NaCl, dried with $MgSO_4$, and filtered. The solvent was removed by rotary evaporation to give the methyl ester, which was subsequently dissolved in 20 mL of dichloromethane. The resulting solution was added dropwise, over 5 min, to a stirred suspension of pyridinium chlorochromate (6.67 g, 30.9 mmol) in 100 mL of dichloromethane. The mixture was stirred at room temperature for 2 h and was then diluted with 200 mL of diethyl ether. The organic solution was decanted from the flask, and the remaining black residue was rinsed thoroughly with two more volumes of diethyl ether. The organic portions were combined and filtered through Florisil to give a clear and

colorless solution. The solvent was removed by rotary evaporation to give methyl 16-oxohexadecanoate (5.21 g, 18.3 mmol, 99% yield). ^{1}H NMR (300 MHz, $CDCl_3$): δ 9.74 (t, J = 1.2 Hz, 1 H), 3.64 (s, 3 H), 2.40 (td, J = 7.5 Hz, J = 1.2 Hz, 2 H), 2.36 (t, J = 7.5 Hz, 2 H), 1.74–1.53 (m, 4 H), 1.40–1.20 (m, 20 H).

A dimesylate ion solution was prepared by suspending sodium hydride (0.58 g, 24.0 mmol) in 5 mL of dimethylsulfoxide (DMSO) at 60° C. Methyltriphenylphosphonium bromide (8.90 g, 25.0 mmol) was dissolved in 25 mL of DMSO, and the resulting solution was added to the dimesylate ion solution at 40° C. After stirring for 30 min, the mixture was diluted with 30 mL of tetrahydrofuran (THF) and was combined with a solution of methyl 16-oxohexadecanoate (5.21 g, 18.3 mmol) in 10 mL of THF. The reaction mixture was stirred at 40° C for 3 h. Water (100 mL was added and the mixture was extracted with diethyl ether (3 × 100 mL). The combined organic portions were washed with 100 mL of water and satd aq NaCl, dried with $MgSO_4$, and filtered. The solvent was removed by rotary evaporation. The crude product was purified by column chromatography on silica gel (9:1, hexanes:diethyl ether) to give methyl 15-hexadecenoate (2.17 g, 7.68 mmol, 42% yield). ^{1}H NMR (300 MHz, $CDCl_3$): δ 5.88–5.74 (m, 1 H), 5.03–4.89 (m, 2 H), 3.67 (s, 3 H), 2.30 (t, J = 7.2 Hz, 2 H), 2.08–1.99 (m, 2 H), 1.64–1.55 (m, 4 H), 1.43–1.18 (m, 20 H).

Methyl 15-hexadecenoate (1.90 g, 6.73 mmol), perfluorodecyl iodide (5.21 g, 8.07 mmol), and the radical initiator 2,2'-azobisisobutyronitrile (AIBN; 0.05 g, 0.32 mmol) were placed into a 25-mL Schlenk flask. The flask was sealed, evacuated until the reactants began to effervesce, and refilled with argon. This process was repeated two additional times. After evacuating the flask a final time, the reaction mixture was heated to 90° C and stirred for 3 h. The flask was then cooled to room temperature, and another portion of AIBN (0.05 g, 0.32 mmol) was added. The aforementioned evacuation process was repeated, and the evacuated flask was again stirred at 90° C for 3 h. These additions of radical initiator were performed at 3-h intervals until all of the methyl 15-hexadecenoate was consumed, as indicated by ^{1}H NMR spectroscopy. The flask was then cooled to room temperature, and the reaction mixture was dissolved with a mixture of 20 mL of THF and 40 mL of acetic acid. Zinc dust (2.50 g, 38.2 mmol) was added to the flask, and the reaction mixture was stirred for 12 h at room temperature. The mixture was then filtered through Celite to give a clear solution. The Celite was rinsed with two 100-mL portions of diethyl ether, and these ethereal rinses were combined with the clear solution. The solvent was removed by rotary evaporation, and the residue was dissolved in 200 mL of diethyl ether. The ethereal solution was rinsed with equivalent volumes of satd aq $NaHCO_3$ and satd aq NaCl, dried with $MgSO_4$, and filtered. After removing the solvent by rotary evaporation, the crude product was purified by column chromatography on silica gel (9:1, hexanes:diethyl ether) to give methyl 17-perfluorodecylheptadecanoate (2.18 g, 2.72 mmol, 40% yield). ^{1}H NMR (300 MHz, $CDCl_3$): δ 3.66 (s, 3 H), 2.30 (t, J = 7.5 Hz, 2 H), 2.15–1.90 (m, 2 H), 1.65–1.50 (m, 4 H), 1.39–1.12 (m, 24 H).

A solution of methyl 17-perfluorodecylheptadecanoate (2.18 g, 2.72 mmol) in 50 mL of THF was added, over 5 min, to a suspension of lithium aluminum hydride (0.30 g, 7.91 mmol) in 100 mL of THF. The mixture was stirred and refluxed under argon for 2 h, cooled to 0° C, and neutralized by dropwise addition of methanol until the evolution of hydrogen ceased. After adding 150 mL of water, concd HCl was added dropwise until the aqueous layer was acidic, as indicated by litmus paper. The mixture was extracted with diethyl ether (3 × 100 mL). The organic portions were combined, rinsed with 100 mL of water, satd aq $NaHCO_3$, and satd aq NaCl, dried with $MgSO_4$, and filtered. After removing the solvent by rotary evaporation, the crude product was purified by column chromatography on silica gel (2:1, hexanes:diethyl ether) to give 17-perfluorodecyl-1-heptadecanol (2.05 g, 2.65 mmol, 97% yield). ^{1}H NMR (300 MHz, $CDCl_3$): δ 3.64 (t, J = 6.6 Hz, 2 H), 2.15–1.92 (m, 2 H), 1.64–1.48 (m, 5 H), 1.40–1.21 (m, 26 H).

17-Perfluorodecyl-1-heptadecanol (2.05 g, 2.65 mmol) was dissolved in a mixture of 50 mL of THF and 150 mL of hexanes. Triethylamine (0.80 g, 7.95 mmol) and methanesulfonyl chloride (0.61 g, 5.30 mmol) were added to the stirred solution, and the reaction mixture was stirred at room temperature for 2 h. After adding 200 mL of water, the organic layer was separated, rinsed with 100 mL of water and satd aq NaCl, dried with $MgSO_4$, and filtered. The solvent was removed by rotary evaporation to give the crude mesylate, which was subsequently dissolved in a mixture of 50 mL of THF and 150 mL of absolute ethanol. Potassium thioacetate (0.59 g, 5.20 mmol) was added to the solution, and the mixture was stirred and refluxed for 2 h under argon. The reaction was then cooled to room temperature and mixed with 200 mL of water. The mixture was extracted with hexanes (3 × 150 mL). After combining the organic portions, the solution was rinsed with 100 mL of satd aq NaCl, dried with $MgSO_4$, and filtered. The solvent was removed by rotary evaporation to give the crude thioacetate, which was subsequently dissolved in 50 mL of THF. This solution was added, over 5 min, to a suspension of lithium aluminum hydride (0.50 g, 13.2 mmol) in 100 mL of THF. The mixture was stirred at 60° C for 2 h under argon, and was then cooled to 0° C and neutralized with methanol. After adding 150 mL of water, conc HCl was added until the aqueous layer was acidic. The organic layer was isolated, rinsed with 100 mL of water, satd aq $NaHCO_3$, and satd aq NaCl, dried with $MgSO_4$, and filtered. The solvent was removed by rotary evaporation, and the crude product was purified by column chromatography on silica gel (hexanes) to give 17-perfluorodecyl-1-heptadecanethiol (2.01 g, 2.54 mmol, 96% yield). Comprehensive analytical data are provided for this final product: (18,18,19,19,20,20,21,21,22,22,23,23,24,24,25,25,26,26,27,27,27-heneicosafluoro-1-heptacosanethiol, F10H17SH). ^{1}H NMR (300 MHz, $CDCl_3$): δ 2.50 (q, J = 7.2 Hz, 2 H), 2.19–1.91 (m, 2 H), 1.74-1.52 (m, 4 H), 1.49–1.25 (m, 27 H). ^{13}C NMR (75.5 MHz, $CDCl_3$): δ 120–110 (bm, 10 C), 34.28, 31.15 (t, $^2J_{CF}$ = 23 Hz), 29.71 (m, 8 C), 29.88, 29.45, 29.35, 29.30, 28.61, 24.88, 20.34. Broad resonances with chemical shifts in the range of δ 120–110 are characteristic of long perfluorocarbon chains.[26] Anal. Calc for

$C_{27}H_{35}F_{21}S$: C, 41.02; H, 4.46. Found: C, 41.03; H, 4.06.

The substrates were titanium-primed (≈5 nm) polished single-crystal silicon (100) wafers covered by 200- or 100-nm-thick polycrystalline gold or silver films of 99.99% purity. Such films are commonly used as substrates for AT SAMs. They predominantly exhibit the (111) orientation, which is, in particular, supported by the observation of the characteristic forward-scattering maxima in the angular distributions of the Au 4f and Ag 3d photoelectrons.[27] The grain size of the Au and Ag films is 20–50 nm, as observed by AFM. The SFAT SAMs were prepared by immersion of the substrates for 24 h at room temperature in 1 mmol SFAT solutions in analytical grade dichloromethane. After immersion, the films were rinsed with dichloromethane and blown dry with pure nitrogen. Extensive characterization showed no evidence for impurities or oxidative degradation products, except for the F10H2S/Ag, where a small amount of silver surface oxide (less than 0.1 ML with respect to the sulfur head groups) was detected.

The SFAT SAMs were characterized by IRRAS, XPS, and NEXAFS spectroscopy. All measurements were performed at room temperature. The XPS and NEXAFS experiments were carried out at a base pressure better than $2 \cdot 10^{-9}$ mbar. Special attention was paid to the data reproducibility and reliability: The experiments were performed several times and with different samples. XPS results were reproduced with two different experimental setups.

Infrared adsorption measurements were performed with a dry-air-purged Bio-Rad FTIR spectrometer Model FTS 175C equipped with a liquid-nitrogen-cooled MCT detector. All spectra were taken with p-polarized light with a PIKE advanced grazing angle accessory at a fixed incident angle of 80° with respect to the surface normal. The measurements were carried out in the range of 650-4000 cm^{-1} at a resolution of 2 cm^{-1} and with at least 1000 scans per spectrum. The spectra are reported in absorbance units $A = -\log R/R_0$, where R and R_0 are reflectivities of the sample and reference, respectively. As a reference, we used SAMs of perdeuterated *n*-eicosanethiols, whose C-D absorption bands at 2050–2200 cm^{-1} do not interfere with the spectral region of interest.[28]

The XPS measurements were performed with a Leybold–Hereaus LHS-12 system and a home-built spectrometer equipped with a VG CLAM 2 analyzer. A normal emission geometry, a Mg K_α X-ray source, and a multichannel detection were used in both cases. The energy scale for the films on gold and the work functions of the spectrometers were referenced to the Au $4f_{7/2}$ peak at 84.0 eV,[29] which resulted in a binding energy (B.E.) of 368.1 eV for the Ag $4d_{5/2}$ peak in agreement with refs 29 (368.3 eV) and 30 (367.9 eV). For all samples, a wide scan spectrum and F 1s, O 1s, C 1s, S 2p, and Au 4f (for Au) or Ag 3d (for Ag) narrow scan spectra were measured. The energy resolution for the C 1s, S 2p, and Au 4f regions was about 0.9 eV.

The spectra acquired with the LHS-12 system were taken as measured, whereas the spectra recorded with the home-built spectrometer were normalized to the total electron yield (TEY) to correct for small differences in sample positions and X-ray intensities typical for this spectrometer. Both experimental procedures resulted in essentially the same spectra for all samples investigated, which justifies the TEY normalization procedure (see also refs 31 and 32) for the home-built apparatus. The spectra were fitted by using a Shirley-type background[33] and symmetric Voigt functions.[34] To fit the S $2p_{3/2,1/2}$ doublet, we used two Voigt peaks with the same FWHM and Gauss/Lorentz proportion, a standard[29,30] spin-orbit splitting of 1.2 eV, and a fixed $S2p_{3/2}/S2p_{1/2}$ intensity ratio of 2.

The NEXAFS measurements were performed with linear polarized light using the HE-TGM 2 monochromator[35] at the German synchrotron radiation facility BESSY-1. The spectra were recorded at the C 1s absorption edge in the partial-yield detection mode with a retarding voltage of –150 V. The energy resolution was ≈0.65 eV. The incidence angle of the linear polarized light was varied from 90° (the **E**-vector in the surface plane) to 20° (the **E**-vector near the surface normal) in steps of 10°–20° to monitor the orientational order within the SFAT films.[36]

The raw NEXAFS spectra were corrected for the energy dependence of the incident photon flux by division through a spectrum of a clean, freshly-sputtered gold sample. For the films on silver, the spectrum of a clean silver sample was subtracted from the SFAT/Ag spectrum before this correction.[32] After the flux correction, the spectra were normalized to the adsorption edge height. For absolute energy calibration, the simultaneously measured photoabsorption signal of a carbon-covered gold grid with a characteristic resonance at ≈285 eV was used. This resonance was separately calibrated to the significant π*-resonance of a graphite sample (HOPG) at 285.38 eV.[37]

3. RESULTS

3.1. XPS measurements

The C 1s and F 1s XP spectra of F10H2SH, F10H11SH, and F10H17SH adsorbed on Au and Ag are shown in Fig. 1. The S 2p XP spectra of these films are presented in Fig. 2. The F 1s intensity is scaled down by the same factor for all spectra in Fig. 1 to allow a direct comparison with the C 1s XP curves. The slightly lower (than for SFAT/Ag) signal-to-noise ratio of the C 1s spectra for SFAT/Au stems from a larger inelastic electron background originated from the Au 4f electrons. The poor signal-to-noise ratio of the S 2p spectra is related to the attenuation of the corresponding signal by the overlayer and the short acquisition time selected to reduce possible X-ray induced damage during the measurement.[38] The positions and the normalized intensities of the F 1s and C 1s emissions are presented in Tables 1 and 2, respectively.

In the spectra in Fig. 2, a single S 2p doublet at B.E. of ≈162.0 eV ($S2p_{3/2}$) for SFAT/Au and ≈161.8 eV (S $2p_{3/2}$) for SFAT/Ag is seen. The B.E.s of these doublets are consistent with thiolate species bonded to the surfaces of gold and silver, respectively.[17,39] The positions and FWHM (1.1 eV) of the S $2p_{3/2}$ and S $2p_{1/2}$ peaks are essentially the same as for normal AT SAMs.

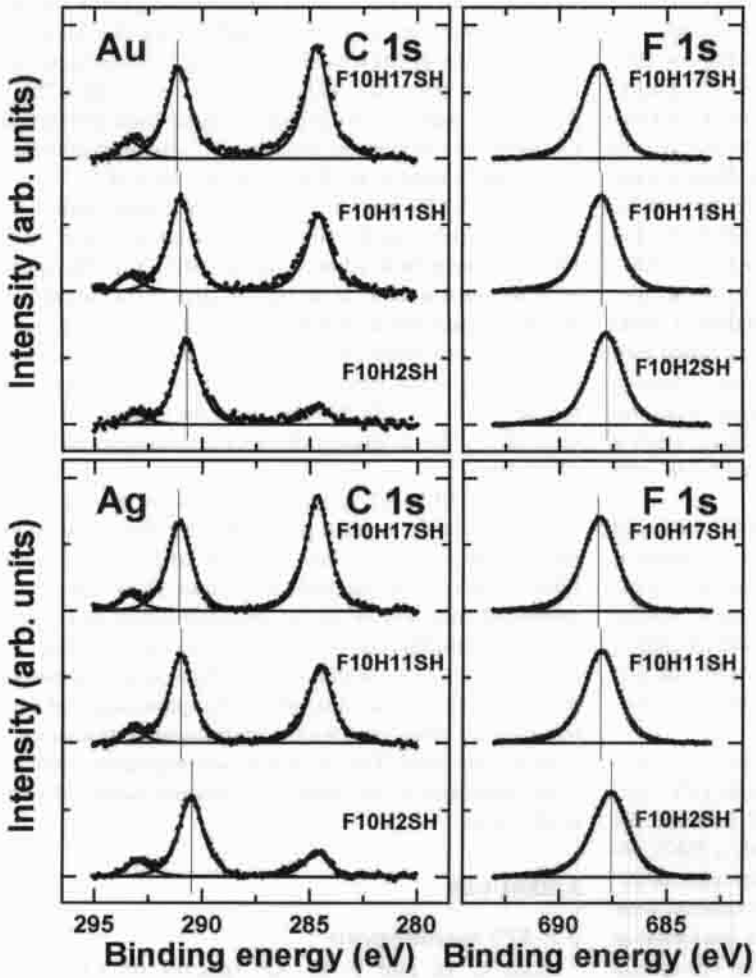

Fig. 1. The C 1s and F 1s XP spectra of F10H2SH, F10H11SH, and F10H17SH on Au and Ag. The observed emission maxima are assigned in the text. The binding energy (B.E.) shift of the emission maxima related to the fluorocarbon chain is highlighted by the thin vertical lines.

Thus, the S 2p XP spectra indicate the presence of only one sulfur species and suggest strong bonding of the SFAT molecules to the substrate via their sulfur head group upon adsorption.

The observed trend in the intensities of the S 2p doublet agrees rather well with the expected attenuation of the respective photoelectrons for the intact SFAT molecules bonded to the substrate via the sulfur head group. In fact, these intensities decrease with increasing film thickness, which is especially pronounced upon comparison of the S 2p emission for F10H2S/Au and F10H2S/Ag with those for the SFAT films with longer hydrocarbon chain.

Adsorption of intact SFAT molecules is confirmed by the C 1s and F 1s XP spectra in Fig. 1. In the C 1s spectra, the emission maxima related to CF_3, CF_2, and CH_2 entities (B.E. of 293.1 eV, 290.7 eV, and 284.7 eV, respectively, for F10H2S/Au) can be easily distinguished. The CH_2-related peaks for F10H2S/Au and F10H2S/Ag are distinctively asymmetric. This could originate from the splitting of the C $1s_{CH_2}$ peak associated with different chemical environments of the two CH_2 entities in F10H2S/Au and F10H2S/Ag, which are bonded either to sulfur or the CF_2-chain. In the SFAT films with a longer hydrocarbon chain, the C $1s_{CH_2}$ emission from the methylene groups in the interior of the hydrocarbon chain dominates the signal. In agreement with the expected compositions of the SFAT SAMs, the intensity of the CH_2-related maximum increases with increasing length of the hydrocarbon part, whereas the intensities of the CF_3- and CF_2-related maxima remain approximately constant (see Table 2). The intensities of C $1s_{CH_2}$ peaks for the same SFAT on Au and Ag are almost equal, which implies a substrate-independent packing density of the hydrocarbon chains, assuming that the attenuation of the C $1s_{CH_2}$ signal by the fluorocarbon part is the same for both substrates. The observed increase of the C $1s_{CH_2}$ intensity on going from the SFAT SAM with two methylene groups in the hydrocarbon chain to those with eleven and seventeen CH_2

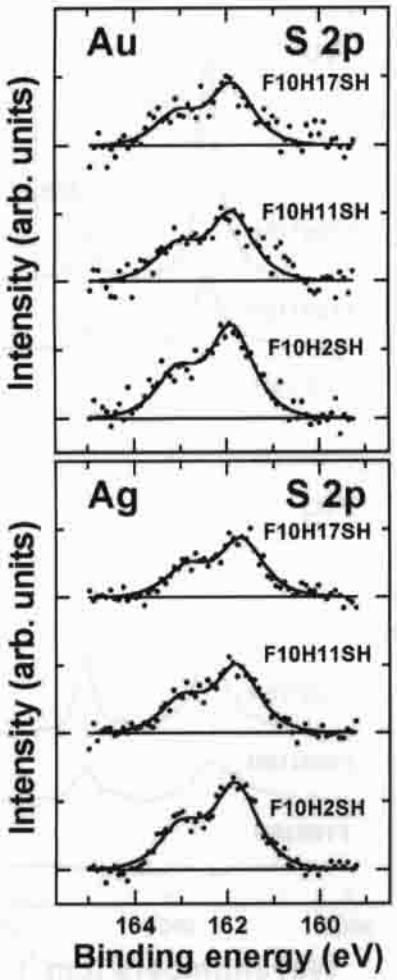

Fig. 2. The S 2p XP spectra of F10H2SH, F10H11SH, and F10H17SH on Au and Ag. The observed emission structures are fitted by a doublet of Voigt peaks with fixed intensity ratio of S $2p_{3/2}$/S $2p_{1/2}$ = 2 and an energy separation of 1.2 eV.

units correlates with the expected proportion $I_{H2} : I_{H11} : I_{H17} = [1 - \exp(-d_{H2}/l)] : [1 - \exp(-d_{H11}/l)] : [1 - \exp(-d_{H17}/l)]$, where d_{Hn} is the assumed thickness of the hydrocarbon part in SAMs formed from F10HnSH and l is the standard attenuation length in AT SAMs (27.3 Å for C 1s with a Mg K_α X-ray source[20,28]). This proportion follows from the general expression for the C $1s_{CH_2}$ intensity $I_{Hn} \sim \exp(-d_{F10}/\lambda_F) \times [1 - \exp(-d_n/\lambda)]$, where d_{F10} and λ_F are thickness of the fluorocarbon part and the attenuation length in a perfluoro-AT SAM, respectively. Considering that λ_F is not known exactly, we prefer to deal with intensity relations rather than absolute values.

Along with the observed behavior of the C $1s_{CF_2+CF_3}$ maxima, similar intensities of the F 1s emission peak (B.E. of 687.9–688.2 eV) are observed in the F 1s XP spectra for all three investigated SFAT SAMs on both substrates (see Table 2). The intensities of F 1s and C $1s_{CF_2+CF_3}$ peaks are not affected by the hydrocarbon part and can be directly related to the packing density of the fluorocarbon chains, which subsequently defines the density in the entire film. We observe the same lateral density in all investigated SFAT SAMs regardless of the substrate and the length of the hydrocarbon chain. A closer inspection reveals that the intensities of the F 1s and C $1s_{CF_2+CF_3}$ emission maxima for the SFAT SAMs of this study vary not more than 6–7%. Thus, a possible difference of the 2D-lattice constant on Au and Ag does not exceed 3–3.5% (≈0.2 Å).

The positions of the C 1s emission maxima related to the CF_3 and CF_2 entities and the position of the F 1s emission peak depend on the composition of the SFAT molecule (see Table 1). The respective binding energies shift to higher values with increasing hydrocarbon chain length or, in other words, with increasing distance between the core excited carbon or fluorine atom and the

Table 1. XPS Peak positions for semifluorinated alkanethiols on gold and silver

	F10HnSH/Au (eV)			F10HnSH/Ag (eV)		
peak	n = 2	n = 11	n = 17	n = 2	n = 11	n = 17
C 1s (CF_3)	293.1	293.3	293.3	293.0	293.2	293.4
C 1s (CF_2)	290.7	291.0	291.1	290.5	291.0	291.1
C 1s (CH_2)	284.7	284.6	284.7	284.7	284.6	284.7
F 1s	687.9	688.1	688.2	687.7	688.1	688.2
S 2p	161.9	161.9	161.9	161.8	161.8	161.7

Table 2. XPS intensities for the hydrocarbon and fluorocarbon parts

	F10HnSH/Au			F10HnSH/Ag		
peak	n = 2	n = 11	n = 17	n = 2	n = 11	n = 17
C 1s (CF_3 + CF_2)	1.00	1.11	1.12	1.00	1.06	1.08
C 1s (CH_2)	0.21	0.86	1.23	0.27	0.85	1.21
F 1s	1.00	1.03	1.00	1.00	1.07	1.05

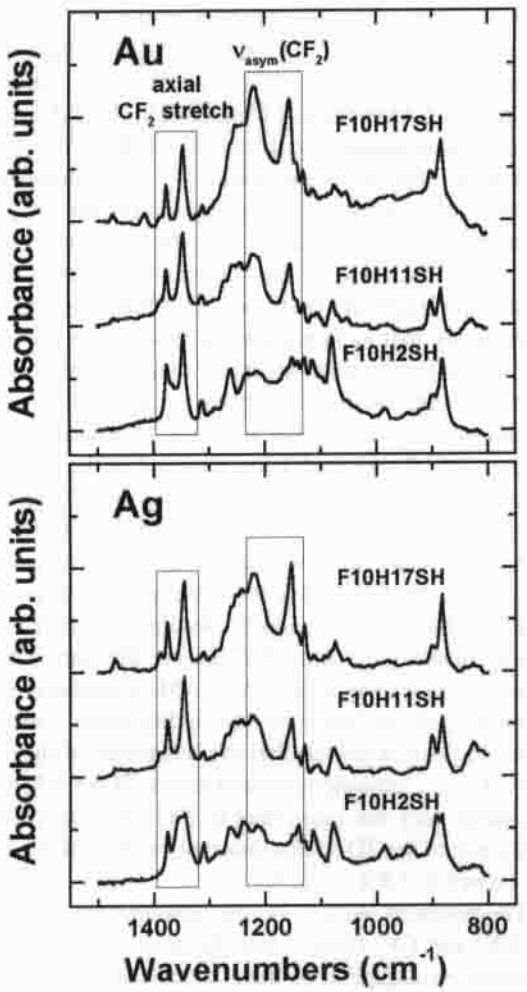

Fig. 3. IR absorption spectra in the CF-stretching region for the SFAT films on gold and silver. The vertical scales in the upper and lower panels are the same.

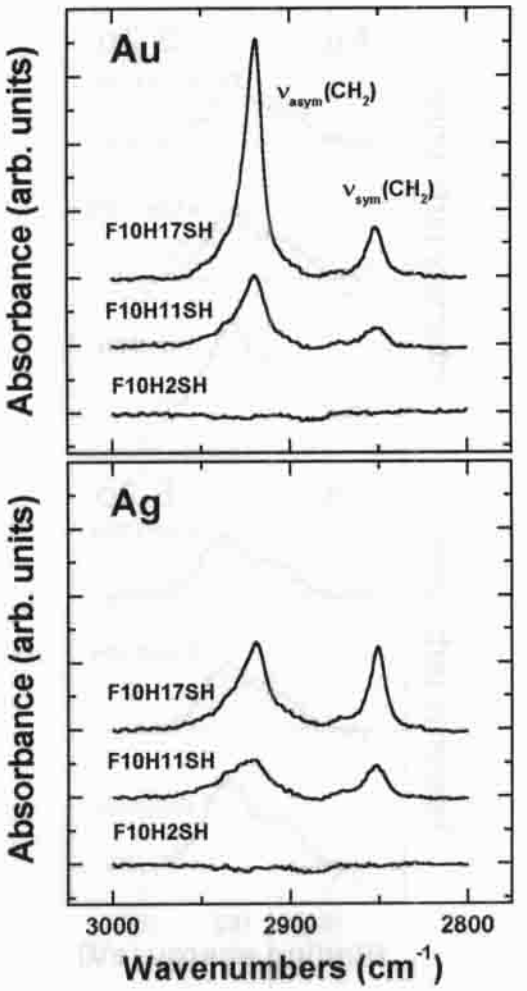

Fig. 4. IR absorption spectra in the C–H-stretching region for the SFAT films on gold and silver. The vertical scales in the upper and lower panels are the same.

substrate. This suggests that the shift is related to final state effects, e.g., to the screening of the photoexcited core hole by the substrate electrons. The extent of screening depends on the distance between the localized hole and the substrate. In this sense, larger F 1s and C $1s_{CF_2+CF_3}$ B.E. shifts with increasing hydrocarbon chain length for SFAT/Ag as compared to SFAT/Au probably indicate a larger thickness of the hydrocarbon part for the films on Ag. A structural transformation of the SFAT films as a function of hydrocarbon chain length could also contribute to the observed change of the F 1s and C $1s_{CF_2+CF_3}$ binding energies, but we have no evidence for drastic structural or conformational changes.

3.2. IRRAS measurements

The IRRAS spectra of the SFAT SAMs on Au and Ag are depicted in Figs. 3 (C–F-stretching region) and 4 (C–H-stretching region). The same absorbance scale is used for the upper (Au) and lower (Ag) panels. The assignment of the observed vibrational modes is provided in Table 3.

The spectral region characterizing the fluorocarbon chains is presented in Fig. 3. This region contains both the stretching and bending modes of the CF_2 groups. The absorption bands at 1375 cm^{-1} and 1346 cm^{-1} are identified as "axial CF_2" stretching vibrations with a strong component of the dynamic dipole moment along the helical axis.[13] These characteristic modes[13] for the helical conformation of the fluorocarbon chain are commonly observed in thin organic films containing these entities.[9,11–13] In our case, these modes are clearly exhibited for all investigated films, which implies that the fluorocarbon parts of the SFAT molecules in the densely packed layers on the Au and Ag substrates retain the helical conformation of the respective bulk materials.

Table 3. Infrared vibrational modes of semifluorinated alkanethiols on gold and silver[a]

mode assignment[b]	F10HnSH/Au (cm^{-1})			F10HnSH/Ag (cm^{-1})			assigned direction of transition dipole moment[b]
	n = 2	n = 11	n = 17	n = 2	n = 11	n =17	
$\nu_{asym}(CH_2)$		2919 vs	2919 m		2919 s	2919 s	⊥ CCC backbone plane
$\nu_{sym}(CH_2)$		2850 s	2851 w		2851 m	2850 m	ip CCC backbone plane,
ip HCH plane							
$\delta(CH_2)$			1471 w			1469 w	
$\delta(CH_2)$			1414 w				
unassigned		1389 sh	1389 sh		1389 sh	1389 w	
$\nu(CF_2)$ progression, axial CF_2 stretch	1375 s	1375 s	1375 s	1375 s	1375 s	1375 s	almost ‖ helical axis
unassigned	1365 sh						
unassigned				1358 s			
$\nu(CF_2)$ progression, axial CF_2 stretch	1346 vs	1346 vs	1346 vs	1346 vs	1346 vs	1346 vs	almost ‖ helical axis
unassigned	1312 m	1312 w	1312 w	1312 m	1312 w	1312 w	
characteristic fingerprint of fluoro-	1272 sh			1272 sh			$\nu_{asym}(CF_2)$ ⊥ helical axis
carbons involving $\nu_{asym}(CF_2)$ and $r(CF_2)$	1262 s		1262 sh	1262 m		1262 sh	
		1257 w	1252 w		1257 w	1252 w	
		1242 w		1240 m	1243 w	1243 w	
	1231 w						
$\delta(CCC)$, $\nu(CC)$, $\nu_{asym}(CF_2) + \nu_{asym}(CF_3)$	1214 w	1218 s	1219 vs	1214 w	1219 w	1219 s	
$\nu_{sym}(CF_2)$, $\delta(CF_2)$	1151 w	1153 s	1155 vs		1154 s	1154 vs	
unassigned	1140 w	1140 sh	1140 sh	1140 m	1140 w	1141 sh	
$\nu(CC)$	1129 m	1129 m	1130 m	1129 w	1129 s	1130 s	
	1115 m	1113 w	1113 w	1114 s	1113 w	1113 w	
		1106 m			1104 w		
	1078 vs	1078 s	1075 w	1079 vs	1077 s	1075 m	
		1051 w	1053 w		1051 w	1053 w	
CF_3	983 m			986 m			
unassigned				943 m			
$\nu(CF_2)$ progression	899 w	901 m	900 m	893 s	900 m	900 m	
$\nu(CF_2)$ progression	881 s	883 s	882 s	882 s	882 s	882 s	

[a]Abbreviations used: ν—stretch, δ—bend, r—rock, w—wag, asym—asymmetric, sym—symmetric, vs—very strong, s—strong, m—medium, w—weak, sh—shoulder, ⊥—perpendicular, ‖—parallel, ip—in plane

[b]References: 9, 12, 13, 17, 63.

The intense adsorption bands in the 1150–1250 cm^{-1} region are also characteristic for fluorocarbon entities. The pronounced bands at ~1220 cm^{-1} and ~1150 cm^{-1} have, in contrast to the axial CF_2-stretches at 1375 cm^{-1} and 1346 cm^{-1}, a significant contribution from the asymmetric CF_2-stretching vibration with a dynamic dipole moment perpendicular to the helical axis.[13] Hence, the relative strength of the axial and asymmetric absorption bands parallel and perpendicular to the helical axis are proportional to the average tilt angle of the fluorocarbon chains. Whereas the intensity of the former vibrational modes remains approximately constant for all three SFAT SAMs on both Au and Ag, the intensity of the latter modes noticeably increases with increasing length of the hydrocarbon chain. On the basis of the surface selection rules,[40] this indicates that the fluorocarbon chains in the SFAT films on both Au and Ag become more tilted with increasing length of the hydrocarbon chains.

The spectral region of the C–H-stretching modes is shown in Fig. 4. The spectra for SAMs formed from F10H11SH and F10H17SH on Au and Ag exhibit distinct asymmetric and symmetric C–H-stretching modes at 2919 cm^{-1} and 2851 cm^{-1}, respectively, related to the CH_2 entities (no noticeable signal in this spectral region is observed for F10H2S/Au and F10H2S/Ag). These band positions are characteristic for the planar zigzag conformation of hydrocarbon chains,[21,41] which is observed for both the respective bulk materials and normal AT SAMs.

Along with information regarding the conformation of the hydrocarbon chains, information about their orientation can be derived from the IR spectra in Fig. 4 by taking into account that the transition dipole moments

of the C–H-stretching modes are perpendicular to the molecular axis, and that the electric field vector of the IR light in the grazing incidence geometry is oriented normal to the substrate. Under these conditions, the observed larger integral intensity of these modes for SFAT/Au as compared to that for SFAT/Ag leads to the conclusion that the hydrocarbon chains in SFAT SAMs on gold are more canted than those on silver. Also, the twist angles of these chains can be extracted from the IR data in Fig. 4. This parameter determines the rotation of the plane containing the zigzag carbon backbone from the plane defined by the chain axis and the surface normal. The twist angle was calculated from the intensity ratio of the asymmetric and symmetric CH_2 C–H-stretching modes following the RATIO method by Debe.[42] This approach indicated twist angles of (54±3)° and (58±3)° for F10H11S/Au and F10H17S/Au, respectively, and (48±3)° and (47±3)° for F10H11S/Ag and F10H17S/Ag, respectively, which are surprisingly close to the corresponding values of 53° and 45° found for normal AT SAMs on gold and silver substrates, respectively.[17]

3.3. NEXAFS measurements

NEXAFS experiments provide information about average orientation of the unoccupied molecular orbitals within the organic film of interest.[36] We first address the electronic structure of SFAT SAMs on the two substrates as a function of the hydrocarbon chain length, as deduced from C 1s NEXAFS spectra acquired at the "magic" X-ray incident angle of 55° (Fig. 5). At this particular experimental geometry, the NEXAFS spectra exclusively reflect the electronic structure of the unoccupied molecular orbitals of the investigated films and are not affected by the angular dependence of the absorption cross-sections.[36]

The spectra in Fig. 5 contain two absorption edges at 287.7–288.0 eV and 293.8–294.1 eV related to the $C_{1s} \rightarrow$ continuum excitations for carbon atoms bonded to hydrogen and fluorine, respectively. The spectra are dominated by the pronounced resonances at ≈292.5 eV, ≈295.5 eV, and ≈299 eV related to the transitions from the C_{1s} state to the C–F σ*, C-C σ*, and C–F′ σ* orbitals of the fluorocarbon part, respectively.[13,43,44] The corresponding transition dipole moments are believed to be oriented almost perpendicular ($C_{1s} \rightarrow$ C–F σ*) or along the chain axis ($C_{1s} \rightarrow$ C–C σ*), respectively.[13,43–45] As to the hydrocarbon part, only a noticeable resonance at ≈288 eV, assigned to the C_{1s} excitations into pure valence C–H orbitals,[36] predominantly Rydberg states,[46,47] or mixed valence/Rydberg states[48] is observed in the spectra for SAMs formed from F10H11SH and F10H17SH. The characteristic C–C * and C–C′ σ* resonances of the hydrocarbon part at ≈293 eV and ≈302 eV, respectively,[22,45,49] overlap with the strong resonances related to the fluorocarbon part and are, therefore, practically indistinguishable. Consequently, only the resonance at ≈288 eV, which we will denote as an R* resonance, is representative for the hydrocarbon part of SFAT SAMs. The orbitals related to this resonance are oriented perpendicular to the alkyl chains axis.[22,45,49]

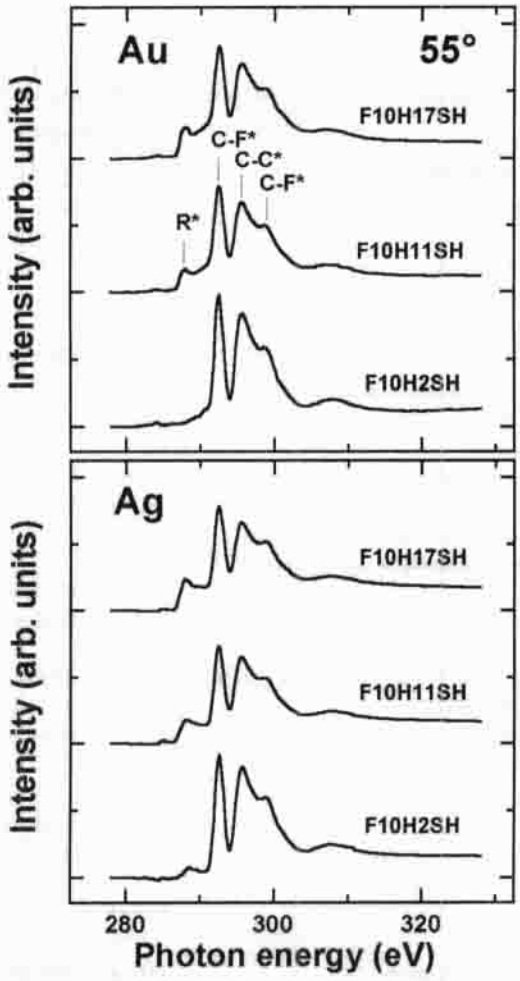

Fig. 5. C 1s NEXAFS spectra of F10H2SH, F10H11SH, and F10H17SH on Au and Ag acquired at an X-ray incident angle of 55°. The characteristic NEXAFS resonances are indicated.

Comparison of the NEXAFS spectra for the SFAT SAMs with different lengths of the hydrocarbon chain shows the expected trend. For both substrates, the intensities of the R* resonance and the C_{1s} (C–H) absorption edge increase with increasing length of the hydrocarbon chain. At the same time, the intensities of the features related to the fluorocarbon chain decrease with increasing length of the hydrocarbon chain. This behavior might appear strange at first glance because the

fluorocarbon part does not change. One has, however, to consider that the spectra in Fig. 5 are normalized to the entire height of the C1s adsorption edge and, subsequently, to the entire number of the carbon atoms in the SFAT molecule. Thus, the decrease of the fluorocarbon-related features stems from the reduction of the relative weight of the fluorocarbon part.

The spectra for the same SFATs on gold and silver are very similar in both the occurrence and intensity of the excitations, except for F10H2S/Au and F10H2S/Ag, where the region of the C_{1s} (C–H) absorption edge and the R* resonance appears different for the two substrates. Whereas the respective features are practically undetectable for F10H2S/Au, a small but pronounced "edge" is observed in this range for F10H2S/Ag. Considering that a small quantity of oxide was detected for the silver surface in F10H2S/Ag (see section 2), we believe that the difference is related to contaminants.

The positions of the resonances related to the fluorocarbon entities and the entire spectral features are very similar to the calculated NEXAFS spectra for poly(tetrafluoroethylene), assuming the standard 13/6 or 15/7 helical conformations of the fluorocarbon chains.[50] The respective calculations, performed with self-consistent spherical muffin-tin potentials and a full multiple-scattering formalism, show a strong dependence of the widths, positions, and intensities of peaks in the NEXAFS spectra on the fluorocarbon chain conformation. Thus, we have further evidence that the fluorocarbon chains in the SFAT SAMs retain the 13/6 or 15/7 helical conformation of the respective bulk materials.

The orientational order in the SFAT films and the average tilt angle of the SFAT molecules can be obtained from the linear dichroism of the NEXAFS spectra, i.e., their dependence on the angle of light incidence.[36] The C1s NEXAFS spectra acquired at the X-ray incidence angles of 90° and 20° are presented in Fig. 6. The intensities of the NEXAFS resonances vary when the angle of X-ray incidence is changed, which implies well-ordered, densely packed SFAT layers on both Au and Ag. The resonances with transition dipole moments oriented along and perpendicular to the fluoro- and hydrocarbon chain axis show an opposite behavior with increasing incidence angle of X-rays. The increase of the R* and C–F σ* resonances and decrease of the C–C σ* resonances suggest a predominantly perpendicular orientation of both the fluoro- and hydrocarbon chains in SFAT SAMs.

The average tilt angles of these chains were derived from the angular dependence of the C–F σ* and R* resonance intensities.[36] The C–F σ* resonance was chosen because of its high intensity and its separation from the other resonances. Moreover, we consciously tried not to consider the C–C σ* resonances because of the existing ambiguity whether the transition dipole moment of these resonances is oriented along the individual C–C bonds[48,49] or along the chain axis[45] (the situation becomes even more ambiguous for a helical chain). The R* resonance was selected as the single distinguishable resonance related to the hydrocarbon part in the present case. The consideration of this resonance provides reasonable structural information in the case of Langmuir–Blodgett films and AT SAMs.[22,31,32,49,51] To extract the intensities of the C-F σ* and R* resonances from the experimental spectra, the whole spectra series were self-consistently fitted by several Gauss peaks representing the observed resonances and by two absorption edges related to the $C_{1s} \rightarrow$ continuum excitations for the hydrogen- and fluorine-bonded carbon atoms.[22,49] The positions and widths of

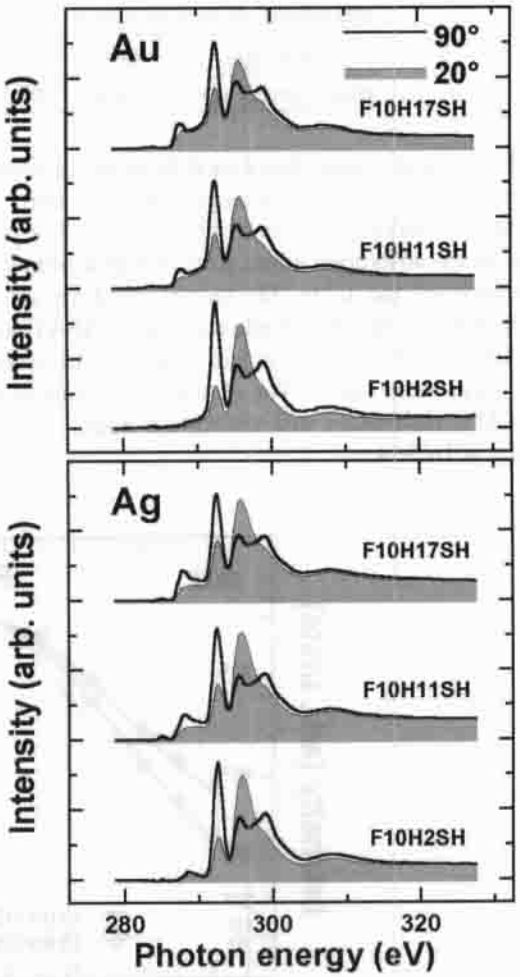

Fig. 6. C 1s NEXAFS spectra of F10H2SH, F10H11SH, and F10H17SH on Au and Ag at normal (90°) and grazing (20°) X-ray incidence. The grazing incidence spectra are shadowed.

Table 4. NEXAFS resonance and absorption edge positions for semifluorinated alkanethiols on gold and silver

resonance/edge	R*	C–F*	C–C*	C–F*	CH-edge	CF-edge
photon energy (eV)	288.0	292.55	295.65	298.8	287.7–288.0	293.8–294.1

the Gauss peaks were determined from the difference spectra ("90°"–"20°") following the procedure described by Outka et al.[49] and Hähner et al.[22] The positions of the absorption edges were obtained from consideration of the C 1s XP spectra, analysis of the NEXAFS spectra of radiation-damaged SFAT/Au,[38] and literature data. The standard shapes of the absorption edges were used.[36] The obtained positions of the NEXAFS resonances and absorption edges are presented in Table 4.

The angular dependences of the R* and C–F σ* resonance intensities for SAMs formed from F10H2SH (circles), F10H11SH (triangles) and F10H17SH (diamonds) on gold and silver are presented in Fig. 7 along with theoretical intensity curves[36] (thin solid lines) for different tilt angles of the hydro- and fluorocarbon chains. We have considered both orbitals as plane ones, which is justified since the R*-orbital is comprised of two mutually perpendicular orbitals (of the s and p character with respect to the C–C backbone plane) with

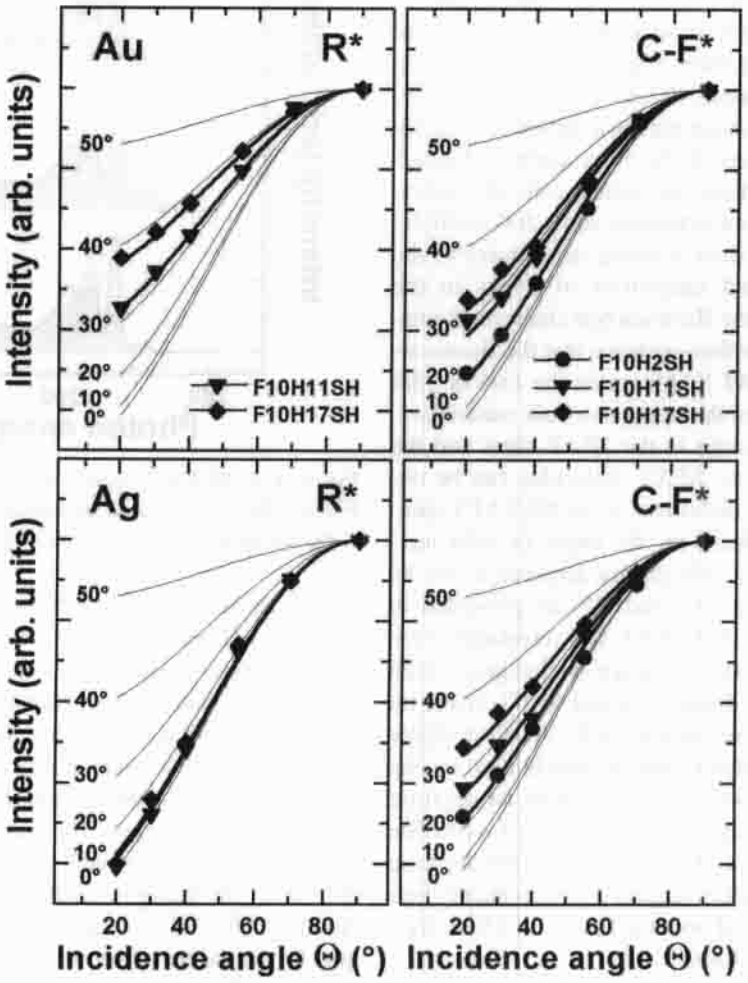

Fig. 7. The angular dependencies of the R* and C–F σ*resonance intensity for F10H2SH (circles), F10H11SH (triangles), and F10H17SH (diamonds) on gold and silver. Also the theoretical dependencies (thin solid lines) for different tilt angles of the hydrocarbon and fluorocarbon chains are presented. The perpendicular orientation of the C–F σ*-orbital with respect to he fluorocarbon chain axis is assumed.

almost identical intensities,[48] and the C–F σ*-orbital can be related to the CF_2 plane in the same manner as the R*-orbital.

The angular dependencies of the C-F σ* resonance intensity give similar tilt angles of the fluorocarbon chains in SFAT SAMs on gold and silver, namely (19±2.5)° for F10H2S/Au and (22±2.5)° for F10H2S/Ag, (28±2.5)° for F10H11S/Au and (27±2.5)° for F10H11S/Ag, and (32±2.5)° for F10H17S/Au and (33±2.5)° for F10H17S/Ag. It should be noted, however, that these values were obtained assuming that the molecular plane of the CF_2 entities is exactly perpendicular to the fluorocarbon chain axis.[13] However, these planes are slightly tilted toward the helix axis, with a tilt angle depending on the helix parameters. Assuming a standard[7–9,52] 15/7 helix with a twist of about 13°–15° per C–C bond for the fluorocarbon chains in the SFAT films, we derive a tilt angle of 8°–9° between the normal of the CF_2 planes and the chain axis. Exactly this angle will be derived from NEXAFS spectra of vertically standing fluorocarbon chains if one assumes that the CF_2 molecular plane is perpendicular to the fluorocarbon chain axis. The real tilt angle of these moieties (0°) is then obtained by a subtraction of the tilt angle of the CF_2 planes from the above value. The situation becomes more complex for a system of almost vertically standing helical chains (as in the present case), but the simple angle subtraction procedure can be used as a rough approximation, which results in the following tilt angles for the fluorocarbon chains: 11° for F10H2S/Au, 14° for F10H2S/Ag, 20° for F10H11S/Au, and 19° for F10H11S/Ag, and 24° for F10H17S/Au, and 25° for F10H17S/Ag. The accuracy of these values is estimated to be ±5°. The source of the error increase with respect to the values derived from Fig. 7 is the uncertainty of the exact form of the helical fluorocarbon chain and the simple angle subtraction procedure used for the correction for the tilt of the CF_2 planes with respect to the chain axis. Note also that the tilt angles for SAMs formed from F10H11SH and F10H17SH may be overestimated by several degrees due to a small contribution from the low-intense (in the present case) C–C σ* resonance of the hydrocarbon chain. This relatively broad resonance located relatively close to the C–F σ* resonance (293 eV and 292.5 eV, respectively) exhibits a reverse linear dichroism with respect to the C-F σ* resonance.

Analysis of the hydrocarbon chain orientation is not affected by these uncertainties because the orientation of the R*-orbitals with respect to the chain axis is well established. A fit of the measured angular dependencies for the R* resonance intensity by the theoretical expressions[36] results in the average tilt angles of 32°±4° and 38°±4° on gold and 10°±4° and 12°±4° on silver for the hydrocarbon chains in SAMs formed from F10H11SH and F10H17SH, respectively. The major source of errors is the relatively (as compared to σ* C–F and σ* C–C) low intensity of the R* resonance and the uncertainty of the location of the C_{1s} (C–H) absorption edge. For F10H2S/Au and F10H2S/Ag, no tilt angles are derived because of the low intensity of the R* spectral feature.

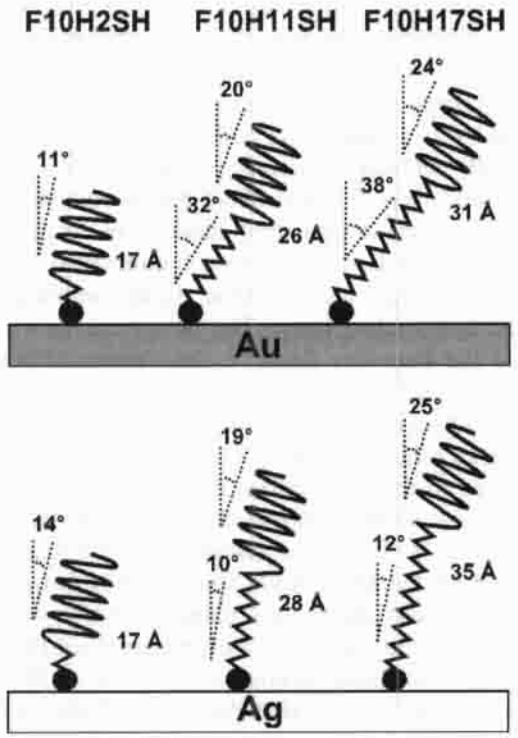

Fig. 8. Schematic drawings of the molecular orientation in F10H2SH, F10H11SH, and F10H17SH on Au and Ag. The average tilt angles of fluoro- and hydrocarbon chains and the entire film thickness are marked.

With the derived tilt angles and assuming a length of 1.3 Å,[53] 1.27 Å,[54] and 1.8 Å[19,55] for CF_2, CH_2, and -S- units, respectively, we can calculate the thicknesses of the SFAT films. The respective values are given in Fig. 8, where schematic drawings of the SFAT molecule orientation in SAMs formed from F10H2SH, F10H11SH, and F10H17SH are depicted. The NEXAFS-derived average tilt angles of fluorocarbon and hydrocarbon chains are also indicated.

4. DISCUSSION

The NEXAFS, IR, and XPS data imply that F10H2SH, F10H11SH, and F10H17SH form well-ordered, densely packed SAMs on polycrystalline gold and silver sub-

strates with predominant (111) orientation. The molecules are bonded to the substrate in the same manner as conventional AT SAMs, as concluded from the observation of a single $S2p_{3/2}/S2p_{1/2}$ doublet in the XP spectra at the same B.E. as that for AT SAMs.

The IR and NEXAFS data imply that both the fluoro- and hydrocarbon chains in SFAT SAMs on both substrates retain the original conformations of the respective bulk materials, i.e., the helical conformation for the fluorocarbon chain and the planar zigzag conformation for the hydrocarbon chain. The IR spectra shown in Figs. 3 and 4 are very similar to those presented in the literature for F10HnS/Au.[9,11]

The helical conformation of the fluorocarbon chain implies an enlarged diameter (5.6 Å) of this moiety as compared to the hydrocarbon chain. Taking into account recent AFM measurements on F10HnS/Au/mica (n = 2, 11, 17),[12,56] a lattice constant of 5.8–5.9 Å can be assumed for the SFAT/Au/Si films used in this study considering also the slightly tilted orientation of the fluorocarbon moieties (note, that the presented IR and XP spectra are almost identical to those for the SFAT/Au/mica films[56,57]). No AFM data are available on the silver substrate, but because of a similar molecular density in all investigated SFAT SAMs on both substrates (as implied by the XPS data), we suggest that the lattice spacing is similar to the one deduced for Au.

The average tilt angle of the fluorocarbon moieties was found to be the same within the error bars for identical SFATs on the Au and Ag substrates. We thus conclude that the substrate does not affect the orientation of the fluorinated tail group. At the same time, both the NEXAFS and IR data suggest that the tilt angle of the fluorocarbon chains in SFAT SAMs strongly depends on the length of the hydrocarbon chain. From the NEXAFS data, this angle is ≈12.5°, ≈20°, and ≈24° for SAMs formed from F10H2SH, F10H2SH, and F10H17SH, respectively. The value of 12.5° for F10H2S/Au practically coincides with the analogous value of ≈12° derived for FnH2S/Au (n = 6, 8, 12) from X-ray diffraction measurements[10] and is close to the value of 20° obtained from the analysis of IR spectra for F8H2S/Au[9] (relevant data for other SFAT SAMs are not available).

The observed trend on going from F10H2S/Au and F10H2S/Ag to the SAMs formed from F10H11SH and F10H17SH can be related to partial disordering of the 2D SFAT arrays with increasing length of the hydrocarbon chain due to increasing mobility of the fluorocarbon part. This hypothesis is supported by a higher disorder of the 2D lattice observed in the AFM images for F10H11S/Au and F10H17S/Au as compared to those for F10H2S/Au.[56] However, the large tilt angle difference for SAMs formed from F10H2SH and F10H11SH and the relatively small change in these parameters for the films fabricated from F10H11SH and F10H17SH suggest that the observed tilt angle increase reflects the influence of the hydrocarbon part.

Contrary to our expectations, the hydrocarbon parts of SFAT SAMs behave differently than the fluorocarbon parts. The average tilt and twist angles of the hydrocarbon moiety are almost independent of its chain length but depend on the substrate, as indicated by the NEXAFS and IR data for SAMs formed from F10H11SH and F10H17SH (the spectral features related to the hydrocarbon chain in F10H2S/Au and F10H2S/Ag are too small to derive any conclusions). Both the twist and tilt angles of the hydrocarbon chains on gold and silver are very close to the respective values for AT SAMs on these substrates. In fact, the average tilt angle of 32°–38° and the twist angle of 54°–58° for F10H11S/Au and F10H17S/Au correlate surprisingly well with the analogous values of 27°–35° and 53° for AT/Au.[17,21-23] Also, the average tilt angle of 10°–12° and the twist angle of 47°–48° for F10H11S/Ag and F10H17S/Ag practically coincide with the respective values of 10°–12° and 45° for AT/Ag.[1,2,17–19]

The observed correlation is unexpected, given that the 2D lattice constant of the SFAT SAMs (≈5.8 Å) is significantly larger than the respective values of ≈5.0 Å for AT/Au and ≈4.7 Å for AT/Ag. Consequently, the intermolecular spacing for the hydrocarbon chains in SFAT SAMs of ≈4.9 Å for SFAT/Au and ≈5.6 Å for SFAT/Ag exceeds their equilibrium vdW distance of 4.4 Å (the intermolecular spacing is equal to the 2D-lattice constant multiplied by the cosine of the respective tilt angle). This should result in a weaker (by a factor of 2–3[16] as compared to AT SAMs) intermolecular interaction between the hydrocarbon chains in the SFAT films, which should lead to a significant difference in the orientation of these moieties for SFAT and AT SAMs. The intermolecular forces are believed to be critical for the entire structure of AT SAMs and, in particular, to be responsible for the different orientation of the alkyl chains on Au and Ag substrates (see Section 1). Thus, we are left to rationalize the orientation of the hydrocarbon chains in the SFAT and AT SAMs on Au and Ag, which appears to be independent of the lateral spacing between the chains. Clustering of the SFAT molecules, resulting in a reduced hydrocarbon chain separation, can be excluded because of topological reasons. An explanation for these unexpected results could be that the interaction of the thiolate head group in both AT and SFAT films with the substrate is the dominant factor determining the tilt and twist angles of the hydrocarbon chains. Such a model would be inconsis-

tent with the generally accepted view that the orientation of the AT molecules on Au and Ag results from the interplay of adsorbate–substrate and adsorbate–adsorbate interactions and that the different orientation of the alkyl chains on these two substrates is related to the vdW interaction between the alkyl chains (see Section 1).[2,19]

Considering the difference in the interchain interaction in AT SAMs and in the hydrocarbon part of SFAT SAMs, we propose that the head-group–substrate interaction strongly influences chain tilt and twist. The thiolate–metal bond is believed to have different strengths for Au and Ag substrates.[17,58] This difference was considered to be the main reason for the different character of thermal desorption of ethanethiol from Ag(110) and Au(110) and the noticeable difference in the cross section of the ion- and electron-induced sulfur desorption from AT SAMs on Au and Ag.[32,59,60] Important in the present context is the proposed difference in the metal–S–C angles for AT SAMs on Au and Ag (104° and 180°, respectively,[1,61,62]), which is related to the sp^3-hybridization of sulfur in AT/Au and sp-hybridization for AT/Ag.[19] The difference in hybridization follows from the energy and orbital shape of the 4d and 5s orbitals of silver and 5d and 6s orbitals of gold participating in the adsorbate–substrate bond.[19] Circumstantial evidence of the predominant role of the adsorbate–substrate interaction for the orientation of AT SAMs is also the observed (9°–16°) change of the alkyl chain tilt angle following exposure of a SAM to a gold substrate with mercury (amalgamation of the gold substrate).[20]

This far, we have discussed either the hydro- or fluorocarbon parts of the SFAT SAMs on Au and Ag. We now consider the complete film structures illustrated in Fig. 8. The orientation of the hydrocarbon chains is, according to our model, determined by the interaction of the thiolate head group with the substrate, whereas the orientation of the fluorocarbon chains seems to be mainly an intrinsic property of the molecules. Different orientations of the hydrocarbon chains in the same SFAT SAMs on Au and Ag do not result in different tilt angles of the fluorocarbon chains. At the same time, the tilt angle of the fluorocarbon moieties depends on the length of the hydrocarbon chain. The different tilt angles of the hydro- or fluorocarbon chains suggest the presence of a kink between the two moieties in the molecule (see Fig. 8).

5. SUMMARY

The structure and conformation of SAMs formed from semifluorinated alkanethiols $CF_3(CF_2)_9(CH_2)_nSH$ with different hydrocarbon chain lengths (n = 2, 11, and 17) on polycrystalline Au and Ag was studied by X-ray photoelectron spectroscopy, infrared reflection absorption spectroscopy, and angle resolved near edge X-ray absorption fine structure spectroscopy. SFATs were found to form highly ordered and densely packed SAMs on both substrates. The molecules are strongly bonded to the substrates via their sulfur head groups, in the same manner as conventional AT SAMs. The hydrocarbon and fluorocarbon moieties of the adsorbed SFATs retain the expected planar zigzag and helical conformation of the respective bulk materials. This implies an enlarged (as compared to AT SAMs) lateral 2D-lattice constant, as indeed observed by AFM (5.9 Å) for F10H11S/Au/mica.[12,56] The orientation of the fluorocarbon chains was found to be independent of the substrate but dependent on the length of the hydrocarbon chain. The average tilt angles of the fluorocarbon chains are (12.5±5)°, (20±5)°, and (24±5)° for SAMs formed from F10H2SH, F10H11SH, and F10H17SH, respectively. Thus, these entities are almost perpendicular to the substrate in F10H2S/Au and F10H2S/Ag but exhibit a slightly larger tilt in SFAT SAMs with longer hydrocarbon moieties.

As alkanethiols on Ag and Au, the hydrocarbon part of the SFAT films exhibits different tilt and twist angles on the two substrates. Surprisingly, these angles were found to be very close to the respective values for AT/Au and AT/Ag: The average tilt angle of 32°–38° and the twist angle of 54°–58° for F10H11S/Au and F10H17S/Au are within errors identical to the corresponding values of 27°–35° and ≈53° for AT/Au, and the average tilt angle of 10°–12° and the twist angle of 47°–48° for F10H11S/Ag and F10H17S/Ag coincide with the respective values of 10°–12° and ≈45° for AT/Ag. Considering the reduced van der Waals interaction between the hydrocarbon chains in the SFAT films (due to the enlarged separation of these chains resulting from the attachment of the bulky fluorocarbon tail groups) as compared to the neat AT SAMs, we suggest that the differences in tilt and twist angles are associated with the different character of the head-group–substrate bonding on Au and Ag.

The experimental results of this study correlate well with the results of previous investigations of SFAT SAMs. The only discrepancy is the average tilt angle of the hydrocarbon chain in F8H11S/Au, which was estimated to be less than that for the conventional AT SAMs in ref 11. However, we believe that the detailed evaluation of the NEXAFS data presented here provides a more accurate value for this parameter than the previous semi-quantitative analysis of IR spectra.[11]

Some questions concerning the SFAT films remain. The detailed arrangement of the SFAT molecules within the two-dimentional layer and the adsorption site(s) of the thiolate head group needs to be determined. A first

attempt of such a structural analysis for FnH2S/Au (n = 5, 7, and 11) was reported by Liu et al.[10]. Also, AFM imaging of the SFAT SAMs on the Ag substrate is highly desirable.

Acknowledgments. We would like to thank the BESSY staff, especially M. Mast for technical help, G. Albert for preparation of the substrates, Ch. Wöll (Universität Bochum) for providing us with experimental equipment, Ph. Harder (Pennsylvania State University) for the help with preliminary IR measurements. This work has been supported by the German Bundesministerium für Bildung, Wissenschaft, Forschung und Technologie through grants No. 05 SF8VHA 1 and 05 SL8VHA 2 and by the Fonds der Chemischen Industrie. The work at the University of Houston was supported by the National Science Foundation (DMR-9700662) and by Seiko Epson Corporation.

REFERENCES AND NOTES

(1) Ulman, A. *An Introduction to Ultra-thin Organic Films: Langmuir-Blodgett to Self-Assembly;* Academic Press: New York, 1991.
(2) Ulman, A. *Chem. Rev.* **1996**, *96*, 1533–1554.
(3) Ulman A. (Ed.), *Thin Films: Self-assembled Monolayers of Thiols*; Academic Press: San Diego, 1998.
(4) Ulman, A.; Eilers, J.E.; Tillman, N. *Langmuir* **1989**, *5*, 1147–1152.
(5) Dixon, D.A.; Van-Catledge, F.A. *Int. J. Supercomputer Appl.* **1988**, *2*, 62–81.
(6) Bunn, C.W.; Howells, E.R. *Nature* **1954**, *174*, 549–551.
(7) Clark, E.S.; Muus, L.T. *Z. Kristallogr.* **1962**, *117*, 119.
(8) Piseri, L.; Powell, B.M.; Dolling, G. *J. Chem. Phys.* **1973**, *58*, 158–171.
(9) Alves C.A.; Porter, M.D. *Langmuir* **1993**, *9*, 3507–3512.
(10) Liu, G-Y.; Fenter, P.; Chidsey, C.E.D.; Ogletree, D.F.; Eisenberger, P.; Salmeron, M. *J. Chem. Phys.* **1994**, *101*, 4301–4306.
(11) Tsao, M.-W.; Hoffmann, C.L.; Rabolt, J.F.; Johnson, H.E.; Castner, D.G.; Erdelen, C.; Ringsdorf, H. *Langmuir* **1997**, *13*, 4317–4322.
(12) Tamada, K.; Nagasawa, J.; Nakanishi, F.; Abe, K.; Hara, M.; Knoll, W.; Ishida, T.; Fukushima, H.; Miyashita, S.; Usui, T.; Koini, T.; Lee, T. R. *Thin Solid Films* **1998**, *329*, 150–155.
(13) Lenk, T.J.; Hallmark, V.M.; Hoffmann, C.L.; Rabolt, J.F.; Castner, D.G.; Erdelen, C.; Ringsdorf, H. *Langmuir* **1994**, *10*, 4610–4617.
(14) Schönherr, H.; Ringsdorf, H. *Langmuir* **1996**, *12*, 3891–3897.
(15) Schönherr, H.; Ringsdorf, H.; Jaschke, M.; Butt, H.-J.; Bamberg, E.; Allinson, H.; Evans, S.D. *Langmuir* **1996**, *12*, 3898–3904.
(16) Taut, C.; Pertsin, A.; Grunze, M. *Langmuir* **1996**, *12*, 3481–3489.
(17) Laibinis, P.E.; Whitesides, G.M.; Allara, D.L.; Tao, Y.-T.; Parikh, A.N.; Nuzzo, R.G. *J. Am. Chem. Soc.* **1991**, *113*, 7152–7167.
(18) Fenter, P.; Eisenberger, P.; Li, J.; Camillone III, N.; Bernasek, S.; Scoles, G.; Ramanarayanan, T.A.; Liang, K.S. *Langmuir* **1991**, *7*, 2013–2016.
(19) Sellers, H.; Ulman, A.; Shnidman, Y.; Eilers, J.E. *J. Am. Chem. Soc.* **1993**, *115*, 9389–9401.
(20) Thome, J.; Himmelhaus, M.; Zharnikov, M.; Grunze, M. *Langmuir* **1998**, *14*, 7435–7449.
(21) Nuzzo, R.G.; Dubois, L.H.; Allara, D. L. *J. Am. Chem. Soc.* **1990**, *112*, 558–569.
(22) Hähner, G.; Kinzler, M.; Thümmler, C.; Wöll, Ch.; Grunze, M. *J. Vac. Technol. A* **1992**, *10*, 2758–2763.
(23) Fenter, P.; Eisenberger, P.; Liang, K.S. *Phys. Rev. Lett.* **1993**, *70*, 2447–2450; Fenter, P.; Eberhardt, A.; Eisenberger, P. *Science* **1994**, *266*, 1216–1218.
(24) Rondestvedt, Jr., C.S.; Thayer, Jr., G.L. *J. Org. Chem.* **1977**, *42*, 2680–2683.
(25) Graupe, M.; Koini, T.; Wang, V.; Nassif, G.M.; Colorado, Jr., R.; Villazana, R.J.; Dong, H.; Miura, Y.F.; Shmakova, O.E.; Lee, T.R. *J. Fluorine Chem.*, **1999**, *93*, 107–115.
(26) Ovenall, D.W.; Chang, J.J. *J. Magn. Reson.* **1977**, *25*, 361–372.
(27) Köhn, F. Ph.D. Thesis, Universität Heidelberg, Germany, 1998.
(28) Harder, P.; Grunze, M.; Dahint, R.; Whitesides, G.M.; Laibinis, P.E. *J. Phys. Chem.* **1998**, *102*, 426–436.
(29) Moulder, J.F.; Stickle, W.E.; Sobol, P.E.; Bomben, K.D. In: *Handbook of X-ray Photoelectron Spectroscopy*; Chastian, J., Ed., Perkin-Elmer Corporation, 1992.
(30) Wagner, C.D.; Riggs, W.M.; Davis, L.E.; Moulder, J.F.; Muilenberg, G. E. *Handbook of X-ray Photoelectron Spectroscopy*; Perkin-Elmer Corporation, 1979.
(31) Zharnikov, M.; Geyer, W.; Gölzhäuser, A.; Frey, S.; Grunze, M. *Phys. Chem. Chem. Phys.* **1999**, *1*, 3163–3171.
(32) Zharnikov, M.; Frey, S.; Heister, K.; Grunze, M. *Langmuir* **2000**, *16*, 2697–2705.
(33) Shirley, D.A. *Phys. Rev. B* **1972**, *5*, 4709-4714.
(34) Wertheim, G.K.; Butler, M.A.; West, K.W.; Buchanan, D.N.E. *Rev. Sci. Instrum.* **1974**, *45*, 1369.
(35) Bernstorff, S.; Braun, W.; Mast, M.; Peatman, W.; Schröter, T. *Rev. Sci. Instrum.* **1989**, *60*, 2097–2100.
(36) Stöhr, J. *NEXAFS spectroscopy*; Springer Verlag: Berlin, 1992.
(37) Batson, P. E. *Phys. Rev. B* **1993**, *48*, 2608–2610.
(38) Frey, S.; Heister, K.; Zharnikov, M.; Grunze, M., Colorado, Jr., R.; Graupe, M.; Shmakova, O.E.; Lee, T.R. *Phys. Chem. Chem. Phys.* **2000**, *2*, 1979–1987.
(39) Himmelhaus, M.; Gauss, I.; Buck, M.; Eisert, F.; Wöll, Ch.; Grunze, M. *J. Electron Spectrosc. Relat. Phenom.* **1998**, *92*, 139–149.

(40) Greenler, R. G. *J. Chem. Phys.* **1966**, *44*, 310–315.
(41) Porter, M.D.; Bright, T.B.; Allara, D.L.; Chidsey, C.E.D. *J. Am. Chem. Soc.* **1987**, *109*, 3559–3568.
(42) Debe, M.K. *J. Appl. Phys.* **1984**, *55*, 3354–3366.
(43) Ohta, T.; Seki, K.; Yokoyama, T.; Morisada, I.; Edamatsu, K. *Phys. Scr.* **1990**, *41*, 150–153.
(44) Castner, D.G.; Lewis, K.B.; Daniel, A.F.; Ratner, B.D.; Gland, J.L. *Langmuir* **1993**, *9*, 537–542.
(45) Hähner, G.; Kinzler, M.; Wöll, Ch.; Grunze, M.; Scheller, M.K.; Cederbaum, L.S. *Phys. Rev. Lett.* **1991**, *67*, 851–854; **1992**, *69*, p. 694 (erratum).
(46) Bagus, P. S.; Weiss, K.; Schertel, A.; Wöll, Ch.; Braun, W.; Hellwig, C.; Jung, C. *Chem. Phys. Lett.* **1996**, *248*, 129–135.
(47) Weiss, K.; Bagus, P.S.; Wöll, Ch. *J. Chem. Phys.* **1999**, *111*, 6834–6845.
(48) Väterlein, P.; Fink, R.; Umbach, E.; Wurth, W. *J. Chem. Phys.* **1998**, *108*, 3313–3320.
(49) Outka, D. A.; Stöhr, J.; Rabe, J. P.; Swalen, J. D. *J. Chem. Phys.* **1988**, *88*, 4076–4087.
(50) Castner, D.L.; Gamble, L.; Fisher, D.A.; Ravel, B. Manuscript in preparation.
(51) Kinzler, M.; Schertel, A.; Hähner, C.; Wöll, Ch.; Grunze, M.; Albrecht, H.; Golzhüter, G.; Gerber, Th. *J. Chem. Phys.* **1994**, *100*, 7722–7735.
(52) Wunderlich, B. *Macromolecular Physics*; Academic Press: New York, 1973.
(53) Brandrup, J.; Immergut, E.H. (Ed.) *Polymer Handbook*; J. Wiley: New York, 1975.
(54) Biebuyck, H.A.; Bain, C.D.; Whitesides, G.M. *Langmuir* **1994**, *10*, 1825–1831.
(55) Dannenberger, O.; Weiss, K.; Himmel, H.-J.; Jäger, B.; Buck, M.; Wöll. Ch. *Thin Solid Films*, **1997**, *307*, 183–191.
(56) Tamada, K.; Fukushima, H.; Colorado, Jr., R.; Graupe, M.; Shmakova, O.E., Lee, T.R.; Ishida, T.; Knoll, W. Manuscript in preparation.
(57) Fukushima, H.; Seki, S.; Nishikawa, T.; Takiguchi, H.; Tamada, K.; Abe, K.; Colorado, Jr., R.; Graupe, O.E.; Lee, T.R. *J. Phys. Chem. B*, in press.
(58) Walczak, M.M.; Chung, C.; Stole, S.M.; Widrig, C.A.; Porter, M.D. *J. Am. Chem. Soc.* **1991**, *113*, 2370–2378.
(59) Jaffey, D.M.; Madix, R.J. *Surf. Sci.* **1994**, *311*, 159–171.
(60) Chenakin, S.P.; Heinz, B.; Morgner, H. *Surf. Sci.* **1999**, *421*, 337–352.
(61) Harris, A.L.; Rothberg, L.; Dubois, L.H.; Levinos, N.J.; Dhar, L. *Phys. Rev. Lett.* **1990**, *64*, 2086–2089.
(62) Lampert, A. Ph.D. Thesis, Universität Heidelberg, Germany, 1997.
(63) Cho, H.-G.; Strauss, H. L., Snyder, R. G. *J. Phys. Chem.* **1992**, *96*, 5290–5295.